



Undrained cyclic behaviors of fiber-reinforced calcareous sand under multidirectional simple shear stress path

Lin Zhou¹ · Jian-Feng Chen¹ · Xiao-Ying Zhuang¹

Received: 8 May 2022 / Accepted: 14 December 2022 / Published online: 6 January 2023
© The Author(s), under exclusive licence to Springer-Verlag GmbH Germany, part of Springer Nature 2023

Abstract

A series of monotonic and multidirectional cyclic simple shear tests were performed on reconstituted fiber-reinforced calcareous sand specimens prepared by the dry deposition method, at a relative density of approximately 50%, considering the effects of fiber contents and cyclic stress levels. The peak shear strength, the linkage between monotonic and cyclic behaviors, liquefaction resistance, and pore pressure responses of calcareous sand with and without fiber reinforcement were analyzed. The results indicate that both unreinforced and fiber-reinforced calcareous sand exhibit limited flow instability behavior and the peak shear strength increases with the increase in fiber content under monotonic loading. The inclusion of fibers and increasing fiber contents can improve the liquefaction resistance of calcareous sand under cyclic loading. A linear relationship was found between the normalized liquefaction resistance of reinforced sand and the number of cycles for triggering liquefaction, and the prediction of liquefaction resistance of fiber-reinforced calcareous sand with various fiber contents can be conveniently achieved according to the linear relationship. The pore pressure prediction model considering the effect of fiber contents was proposed, which was capable of effectively simulating the pore pressure generation of fiber-reinforced calcareous sand.

Keywords Calcareous sand · Fiber · Liquefaction resistance · Multidirectional simple shear tests · Peak shear strength · Pore pressure

1 Introduction

Soil liquefaction threatens the safety of civil engineering structures constructed on sandy ground during an earthquake; thus, geosynthetic reinforcement technology has been widely developed and utilized to reduce the risk of soil liquefaction and improve the performance of backfill materials under seismic loading [10, 65]. Furthermore, with the rapid development of coastal and ocean engineering, calcareous sand has been used as backfill materials in the construction of embankments, retaining structures, slopes,

and subgrade soils, among other soil-related structures [55–57]. Compared to quartz sand, calcareous sand with intra-voids and large inter-particle spaces has a relatively looser structure [64]. Research revealed that saturated calcareous sand has liquefaction potential under undrained conditions [46].

Various planar geosynthetics have been applied in the research of seismic responses of reinforced soils, including studies of geogrid [14, 34, 35, 54], geotextile [13, 18, 51], and steel or polymeric strip [24, 59, 61]. Geogrid can effectively improve the liquefaction resistance of soil by decreasing the development of excess pore pressure [39], indicating that planar geosynthetics have great promise for liquefiable soil treatment. Nevertheless, the defect that cannot restrain potential weak planes that commonly develop parallel to reinforcement materials is obvious for planar geosynthetics [60]. To address this weakness, randomly distributed fibers were used in soil reinforcement. Maheshwari et al. [39] investigated the liquefaction resistance of Solani sand reinforced with various methods (i.e.,

✉ Jian-Feng Chen
jf_chen@tongji.edu.cn

Lin Zhou
sunzourise@126.com

Xiao-Ying Zhuang
xiaoying.zhuang@gmail.com

¹ Department of Geotechnical Engineering, College of Civil Engineering, Tongji University, Shanghai 200092, China

geogrid, geosynthetic fibers, and natural coir fibers) through shaking table tests and concluded that fiber reinforcement offered a better efficiency in reducing the generation of excess pore water pressure and vibration subsidence than geogrid reinforcement.

As it improves the soil performance more than planar geosynthetics, fiber reinforcement attracts the attention of researchers, and considerable efforts have been devoted to evaluating the behaviors of fiber-reinforced soil under static [15, 17, 20, 38, 42] and cyclic loads [3, 5, 16, 62, 63]. For static load, Liu et al. [37] explored liquefaction behaviors of fiber-reinforced sand using undrained ring-shear tests. They reported that the peak shear strength of quartz sand increased with the fiber contents, and the presence of fibers might restrict the occurrence of lateral spreading for loose specimens. A similar conclusion was also obtained by Correia et al. [9] through triaxial compression tests and revealed that the increased soil shear strength can be attributed to the increase in apparent cohesion. However, compared to static load the liquefaction potential of sand will increase dramatically under cyclic load; therefore, investigating the cyclic behaviors of fiber-reinforced sand is more meaningful. Noorzad and Amini Fardad [40] conducted thirty stress-controlled cyclic triaxial tests to discuss the liquefaction resistance and shear modulus of randomly distributed fiber-reinforced quartz beach sand. The results indicated that the liquefaction resistance and shear modulus of sand were improved with increasing fiber content. Behzad Fatahi [3] investigated the behaviors of recycled geofiber-reinforced sand through a series of undrained cyclic triaxial tests and concluded that as recycled geofiber content increased, the liquefaction resistance of sand increased remarkably. Zhang et al. [63] also reported that increasing fiber content and fiber length resulted in a higher liquefaction resistance of quartz sand. Nevertheless, the aforementioned research completely focused on the static and cyclic behaviors of fiber-reinforced quartz sand, and the achieved results of the effect of fiber reinforcement on the behaviors of quartz sand were sufficient. The properties of calcareous sand differ greatly from those of quartz sand; thus, some conclusions on the effect of fiber reinforcement obtained from quartz sand cannot be simply extended to calcareous sand, whereas none of the existing research investigates the cyclic characteristics of fiber-reinforced calcareous sand.

Additionally, the available studies on the cyclic behaviors of fiber-reinforced quartz sand were basically carried out through conventional dynamic triaxial apparatus, which can only apply shear stress in a plane at an angle of 45° to the horizontal plane. However, this loading condition is significantly different from an earthquake loading where the shear stress mainly occurs in the horizontal plane [60]. Fortunately, the deficiency can be overcome by another

type of shear apparatus, that is, the simple shear apparatus. Recently, some seminal studies on the simple shear behaviors of sand have been conducted [23, 27]. For example, Lashkari et al. [28, 29] performed a series of constant volume direct simple shear tests to investigate the effects of particle shape and over-consolidation history on the instability of sand, respectively. Moreover, as the ground moved in more than one horizontal direction during earthquakes, therefore, shear stress applied to soil elements varied not only in shear stress magnitude but also in shear stress direction [52]. Jin and Guo [23] also revealed that the multidirectional loading pattern with a circular stress path was more suitable to reflect in situ stress fields caused by earthquakes. Consequently, to exactly acquire the seismic behaviors of sand reinforced with fibers only based on tests conducted on dynamic triaxial apparatus which can only provide unidirectional loading was insufficient [22]. Nevertheless, the influence of multidirectional loading on cyclic behaviors of fiber-reinforced calcareous sand was completely unknowable and yet to be tested.

This study evaluated the performance of fiber-reinforced calcareous sand through a series of monotonic and multidirectional cyclic simple shear tests. By considering the effects of different cyclic stress ratios and fiber contents, the behaviors of reinforced calcareous sand were investigated, along with the peak shear strength, the linkage between monotonic and cyclic behaviors, liquefaction resistance, and pore pressure. Furthermore, by analyzing available test data obtained from calcareous sand with varying fiber contents, normalized liquefaction resistance, and pore pressure prediction empirical models applicable to fiber-reinforced calcareous sand were proposed.

2 Test procedures

2.1 Test equipment and materials

The variable direction dynamic simple shear apparatus manufactured by Global Digital was used in this test. Figure 1 gives an overall view of the dynamic simple shear apparatus and sectional details of the specimen. As illustrated in Fig. 1, the apparatus can provide one vertical stress (Z direction) and two orthogonal shear stresses (X and Y directions) on a specimen independently. Instead of additional pressure controllers, hydraulic power packs, and control boxes, three encoder-controlled high-precision actuators (including an axial and two horizontal actuators) are used in the dynamic simple shear apparatus, which enables the machine to operate more stably. All actuators can be controlled using position or load control in accordance with the requirements of users. The maximum loads of axial and horizontal actuators are 5 kN and 2 kN,

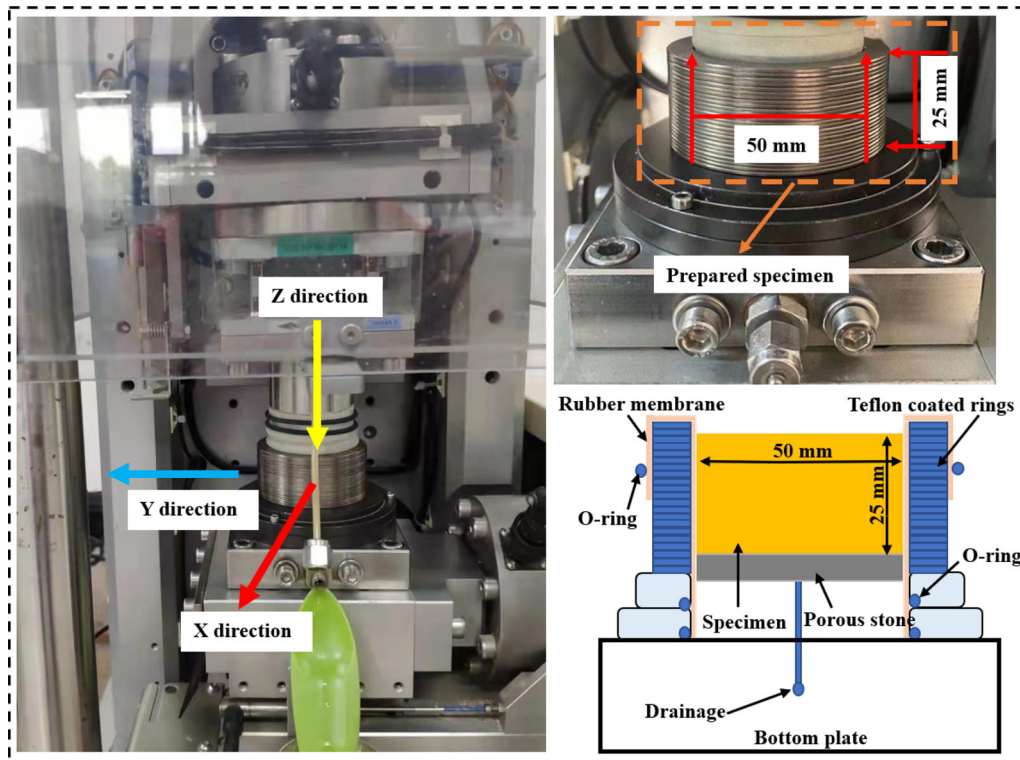


Fig. 1 Overall view of the dynamic simple shear apparatus and sectional details of the specimen

respectively, with an accuracy of less than 0.1% of the full range of axial and horizontal forces. A cylindrical specimen 50 mm in diameter and 25 mm in height was used in this test. To ensure the K_0 condition, 25 low-friction Teflon-coated rings (each ring is 1 mm high) with sufficient stiffness were placed outside the membrane of the specimen, as shown in Fig. 1. More detailed information regarding this apparatus was provided by Li et al. [33].

The soil used in this study to reconstitute the specimens was calcareous sand sampled from the south sea of China (Fig. 2a, b). It is also known as skeletal sand [44], for which the mineral composition is primarily aragonite and high-Mg calcite and the chemical composition is mainly calcium carbonate [6]. The scanning electron microscope (SEM) performed on clean calcareous sand depicts that calcareous sand contains irregular particle shapes and intra-particle voids. Calcareous sand has a coefficient of

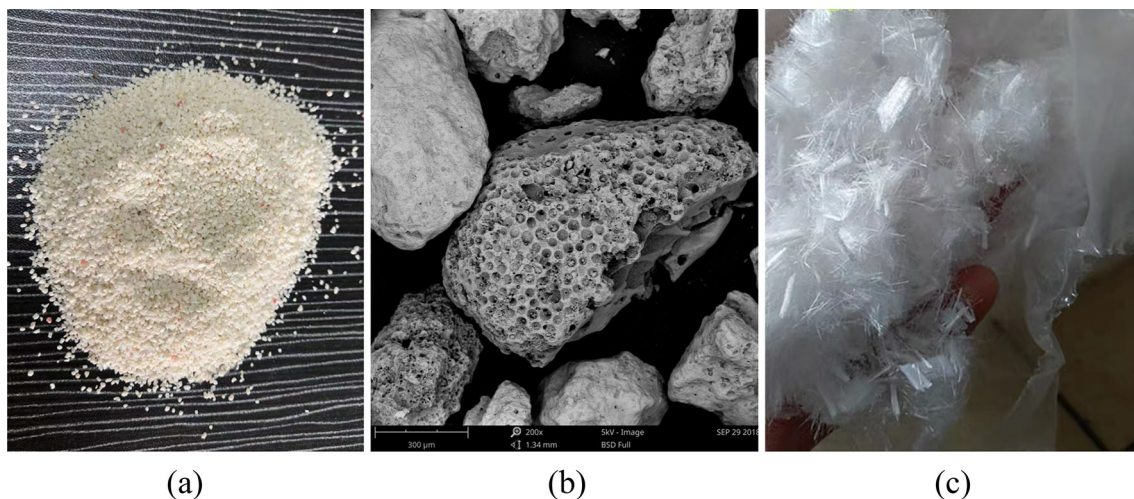


Fig. 2 Test materials: **a** calcareous sand; **b** SEM image of calcareous sand; **c** fiber

uniformity (C_u) and a coefficient of curvature (C_c) of 3.29 and 1.08, respectively. The maximum and minimum void ratios of calcareous sand measured are $e_{\max} = 1.26$ and $e_{\min} = 0.71$, respectively, with a specific gravity of $G_s = 2.85$. As illustrated in Fig. 3, the grain size distribution of calcareous sand tested in this study is classified as susceptible to liquefaction according to PHRI [43].

The average length of the polypropylene fiber used in the current test is 6 mm, and its standard deviation is 0.835, as shown in Fig. 2c. The polypropylene fiber is 0.025 mm in diameter, and has a tensile strength of 550 MPa, elasticity modulus of 4150 MPa, and specific gravity of 0.91. This type of fiber is commonly applied in practical engineering and has also been adopted by other researchers as reinforcement materials for soil due to its satisfactory durability and tensile strength [63].

2.2 Specimen preparation

The required amounts of polypropylene fibers were mixed with calcareous sand using an electric mixer until a uniform soil-fiber mixture was acquired. Subsequently, the soil-fiber mixture was divided into three equal parts, and then, each part was carefully filled into the mold by the dry deposition method [23, 58]. The designed relative density ($D_r = 50\%$) of specimens can be obtained by tapping the side of the mold in a uniform and consistent way [33]. To improve bonding between different layers, slightly scratching the top of each layer before placing the next layer was necessary [4]. During specimen preparation, fiber-reinforced calcareous sand with identical fiber content (ω) was generally prepared in the same batch based on the estimated number of applied cyclic stress ratios (CSR). This approach ensured consistency of specimens at the various CSR and the same ω .

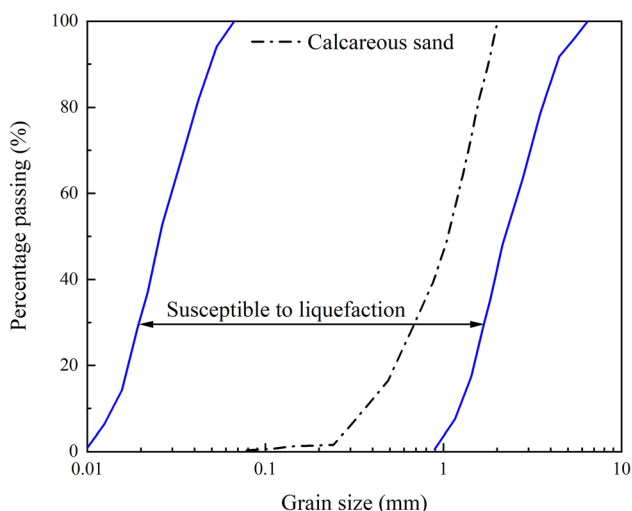


Fig. 3 Grain size distribution of calcareous sand

2.3 Test program

The prepared specimen was placed on the bottom plate of the testing apparatus (Fig. 1). Afterwards, a fixed initial vertical stress ($\sigma'_{v0} = 150$ kPa) was applied to the specimen, and then, a series of undrained monotonic and multidirectional cyclic simple shear tests were performed on unreinforced and fiber-reinforced calcareous sand under constant volume conditions. It was worth noting that all tests were conducted on specimens composed of dry calcareous sand. The variation of σ'_{v0} in a specimen under constant volume conditions is assumed equivalent to the development of excess pore water pressure when a saturated specimen is tested under true undrained conditions [12, 23].

The monotonic tests were performed using a shear strain rate of 0.1 mm/min. The cyclic tests were conducted under a stress-controlled condition with a sinusoidal wave and a frequency of 0.1 Hz. The same frequency can be found in some studies concerning the cyclic behaviors of sand under seismic load [4, 19, 63]. Four different CSR (i.e., CSR = 0.075, 0.094, 0.113, and 0.132) and five ω (i.e., $\omega = w_f/w_s = 0, 0.3, 0.5, 0.8$ and 1%, where w_f and w_s are the weight of fiber and dry calcareous sand, respectively) were used in multidirectional cyclic simple shear tests. Tables 1 and 2 present the test conditions for the undrained monotonic and cyclic simple shear tests performed in this study, respectively. The D_r before the shear tests has been calculated based on the data of soil mass and reduced height of specimens due to the applied σ'_{v0} [28].

Figure 4a depicts applied cyclic shear stress waves of multidirectional loading at different CSR. In this research, CSR is defined as:

$$\text{CSR} = \frac{\sqrt{(\tau_{\text{cyc}})^2 + (\tau_{\text{ycyc}})^2}}{\sigma'_{v0}} \quad (1)$$

Table 1 Summary list of tests in monotonic loading

No. of tests	ω (%)	D_r (%)	σ'_{v0} (kPa)	τ_p (kPa)
Mono- ω 0-1	0	54	50	4.99
Mono- ω 0-2	0	54	150	20.00
Mono- ω 1-1	0.3	53	50	5.48
Mono- ω 1-2	0.3	54	150	21.40
Mono- ω 2-1	0.5	53	50	6.79
Mono- ω 2-2	0.5	52	150	22.60
Mono- ω 3-1	0.8	52	50	7.30
Mono- ω 3-2	0.8	53	150	24.00
Mono- ω 4-1	1	52	50	9.20
Mono- ω 4-2	1	53	150	24.39

τ_p = peak shear strength

Table 2 Summary list of tests in multidirectional cyclic loading

No. of tests	CSR	ω (%)	D_r (%)	σ'_{v0} (kPa)	N_L	N_{Lre}/N_{Lun}
Multi- ω 0-1	0.075	0	54	150	67	–
Multi- ω 1-1	0.075	0.3	53	150	110	1.64
Multi- ω 2-1	0.075	0.5	53	150	152	2.27
Multi- ω 3-1	0.075	0.8	52	150	190	2.84
Multi- ω 4-1	0.075	1	52	150	300	4.48
Multi- ω 0-2	0.094	0	54	150	22	–
Multi- ω 1-2	0.094	0.3	52	150	28	1.27
Multi- ω 2-2	0.094	0.5	53	150	36	1.64
Multi- ω 3-2	0.094	0.8	52	150	45	2.04
Multi- ω 4-2	0.094	1	52	150	68	3.09
Multi- ω 0-3	0.113	0	54	150	10	–
Multi- ω 1-3	0.113	0.3	54	150	12	1.20
Multi- ω 2-3	0.113	0.5	52	150	18	1.80
Multi- ω 3-3	0.113	0.8	52	150	20	2.00
Multi- ω 4-3	0.113	1	52	150	40	4.00
Multi- ω 0-4	0.132	0	53	150	4	–
Multi- ω 1-4	0.132	0.3	52	150	5	1.25
Multi- ω 2-4	0.132	0.5	53	150	7	1.75
Multi- ω 3-4	0.132	0.8	52	150	11	2.75
Multi- ω 4-4	0.132	1	52	150	13	3.25

$N_{Lun} = N_L$ of unreinforced specimens; $N_{Lre} = N_L$ of reinforced specimens

where τ_{xcyc} and τ_{ycyc} denote the maximum values of applied shear stress of X and Y directions, respectively. It can be found that shear stresses with the same amplitude are simultaneously applied to different directions which are perpendicular to each other (i.e., phase difference $\theta = 90^\circ$), inducing a circular stress path (i.e., τ_x versus τ_y in a circular shape, where τ_x and τ_y denote the shear stress of X and Y directions), as shown in Fig. 4b. The recorded acceleration-time histories of the Hyogo-ken Nanbu earthquake in 1995 indicate that the shear strain path applied to soils shows a circular shape during this earthquake; thus, the multidirectional loading with circular stress path is more suitable to reflect in situ seismic stress fields [23]. Furthermore, as noted by Pyke et al. [45], multidirectional shaking could increase settlements to as much as three times the settlements caused by shaking in one direction and reduce the liquefaction resistance of the sand. Analyses that ignore the multidirectional shear effect may lead to unsafe design [52].

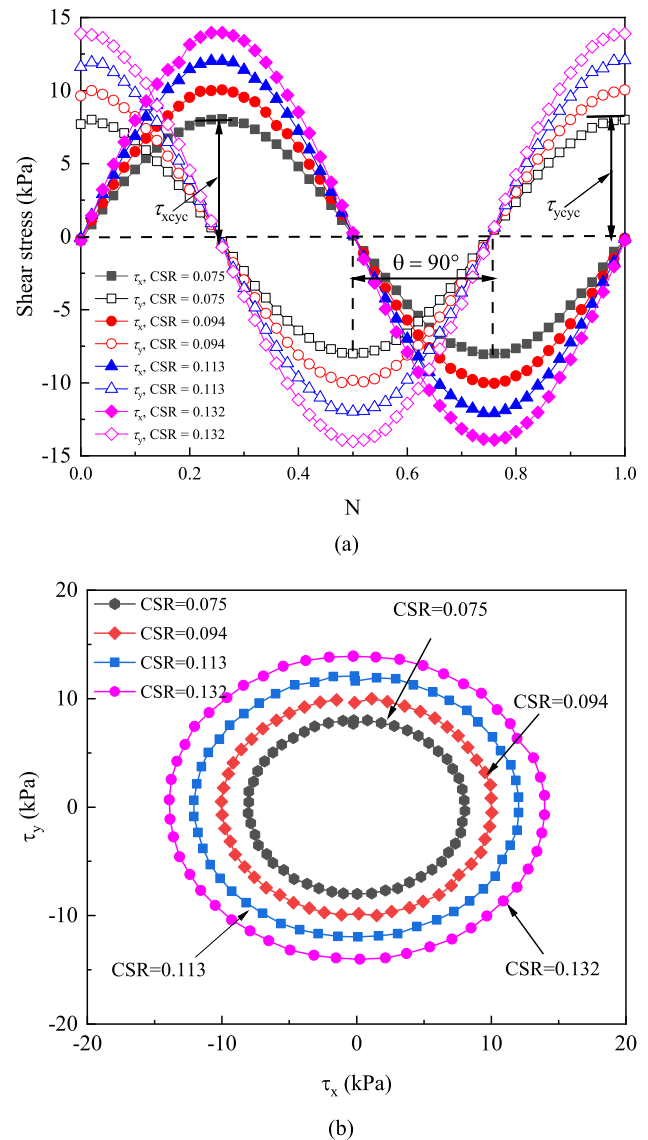


Fig. 4 Schematic of applied cyclic loads: **a** shear stress waves; **b** shear stress paths

3 Results and discussion

3.1 Simple shear behaviors under monotonic loading

Figure 5 depicts the stress–strain curves of the unreinforced and fiber-reinforced calcareous sand under monotonic loading with initial vertical stresses (σ'_{v0}) of 50 and 150 kPa. It can be observed that with the increase of shear strain (γ) the calcareous sand demonstrates a transient post-peak strain softening (shear stress τ reaches a transient peak value at a minor strain and then, drops to its minimum value), whereas the typical strain-hardening behavior is identified in the stress–strain curves during the subsequent monotonic loading. As noted by Lashkari et al. [28], the

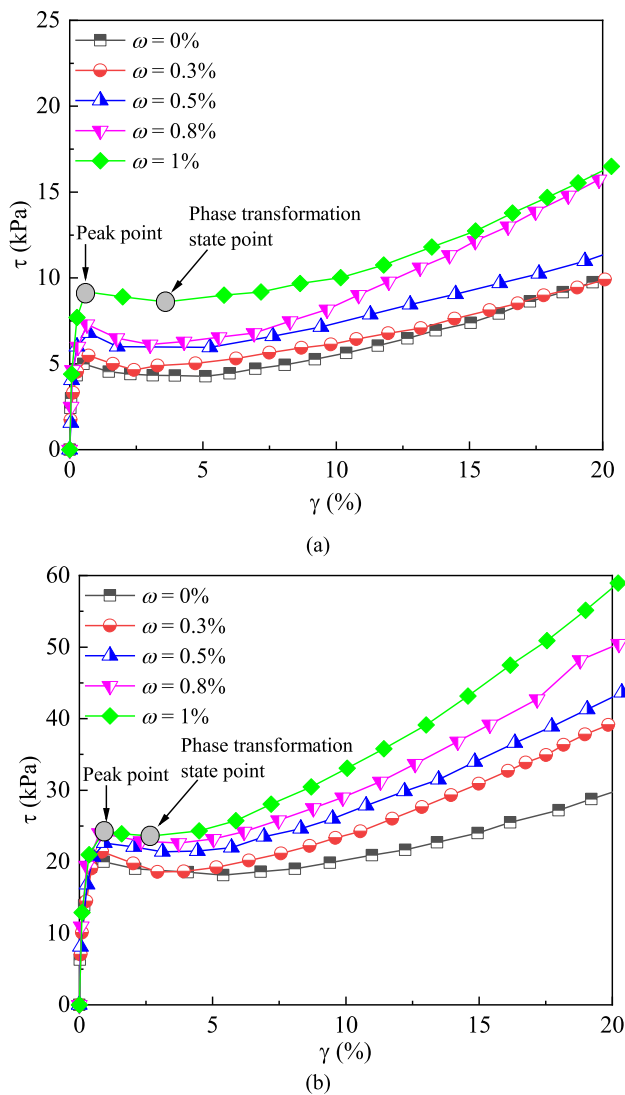


Fig. 5 Comparison of the stress–strain curves of unreinforced and fiber-reinforced calcareous sand under monotonic loading: **a** $\sigma'_{v0} = 50$ kPa; **b** $\sigma'_{v0} = 150$ kPa

mentioned undrained behavior of calcareous sand can be categorized as *limited flow instability* frequently found in specimens with a medium loose state [53]. Furthermore, the inclusion of fiber cannot change the undrained behavior (*limited flow instability*) of calcareous sand, nevertheless, can significantly increase the transient peak shear strength (τ_p) and phase transformation shear strength (τ_{PT}), as illustrated in Fig. 5. Indeed, the similar result that the soil shear strength increases with the increase in fiber content at $\omega \leq 1\%$ is in agreement with the behavior of quartz sand reinforced by recycled carpet fiber as reported by Behzad Fatahi [3]. This is because the interfacial shear stress between fiber and soil particles restrains the slip of soil particles, and the flexible fiber encasing the soil particles can also provide tensile stress to restrict the soil particles

when the soil particles tend to move under monotonic loading [36].

As indicated by the comparison of Fig. 5a, b, when $\sigma'_{v0} = 150$ kPa, the difference in τ_p of calcareous sand with various fiber contents is small, whereas, with the decrease in the σ'_{v0} to 50 kPa, the increase in fiber content will result in a larger distinction in τ_p for calcareous sand. The result demonstrates that the reinforcement efficiency of increasing fiber content in improving shear strength is more pronounced at a smaller σ'_{v0} . A similar conclusion that reinforcement efficiency is more significant at a lower effective confining pressure has also been reported by Boominathan and Hari [4].

3.2 Typical cyclic behaviors

The cyclic pore pressure generation was presented in a normalized form represented by the ratio of pore pressure (u) at a certain number of cycles (N) to σ'_{v0} (i.e., $r_u = u/\sigma'_{v0}$). The onset of sand liquefaction is defined as the pore pressure ratio equal to 1 in this test [48]. N_L is defined as the number of cycles required to achieve soil liquefaction. Typical results of multidirectional cyclic simple shear tests with circular stress path for unreinforced and fiber-reinforced specimens with $\omega = 1\%$ at a CSR value of 0.075 under initial vertical stress of 150 kPa are illustrated in Figs. 6 and 7, respectively. It can be observed that the development curves of shear strain (γ) and pore pressure ratio (r_u) for unreinforced and fiber-reinforced sand are similar, and the main difference is that reinforced sand requires more cycles to reach a liquefaction state. Nevertheless, the shear stress–strain curve (i.e., τ_x versus γ_x , and τ_y versus γ_y , where γ_x and γ_y denote the shear strain of X and Y directions) and orbit of the shear strain (i.e., γ_x versus γ_y) for sand with and without fiber reinforcement exhibit remarkable differences. For unreinforced sand, the deformation sharply increases before reaching the liquefaction state, as shown in Fig. 6c, d. Whereas, fiber-reinforced sand presents a gradual increase in deformation until reaching the liquefaction state, as illustrated in Fig. 7c, d. This is mainly because fibers intersecting with shear failure planes can provide tensile stress to restrict the deformation of the specimen under cyclic loading, and the active load applied on shear failure planes is distributed to a larger area through the tensile stress in fibers, avoiding a sudden increase in deformation.

3.3 Linkage between monotonic and cyclic behaviors

Figure 8a, b show the typical effective stress paths for unreinforced and fiber-reinforced sand with $\omega = 1\%$ under monotonic loading. The effective stress paths develop

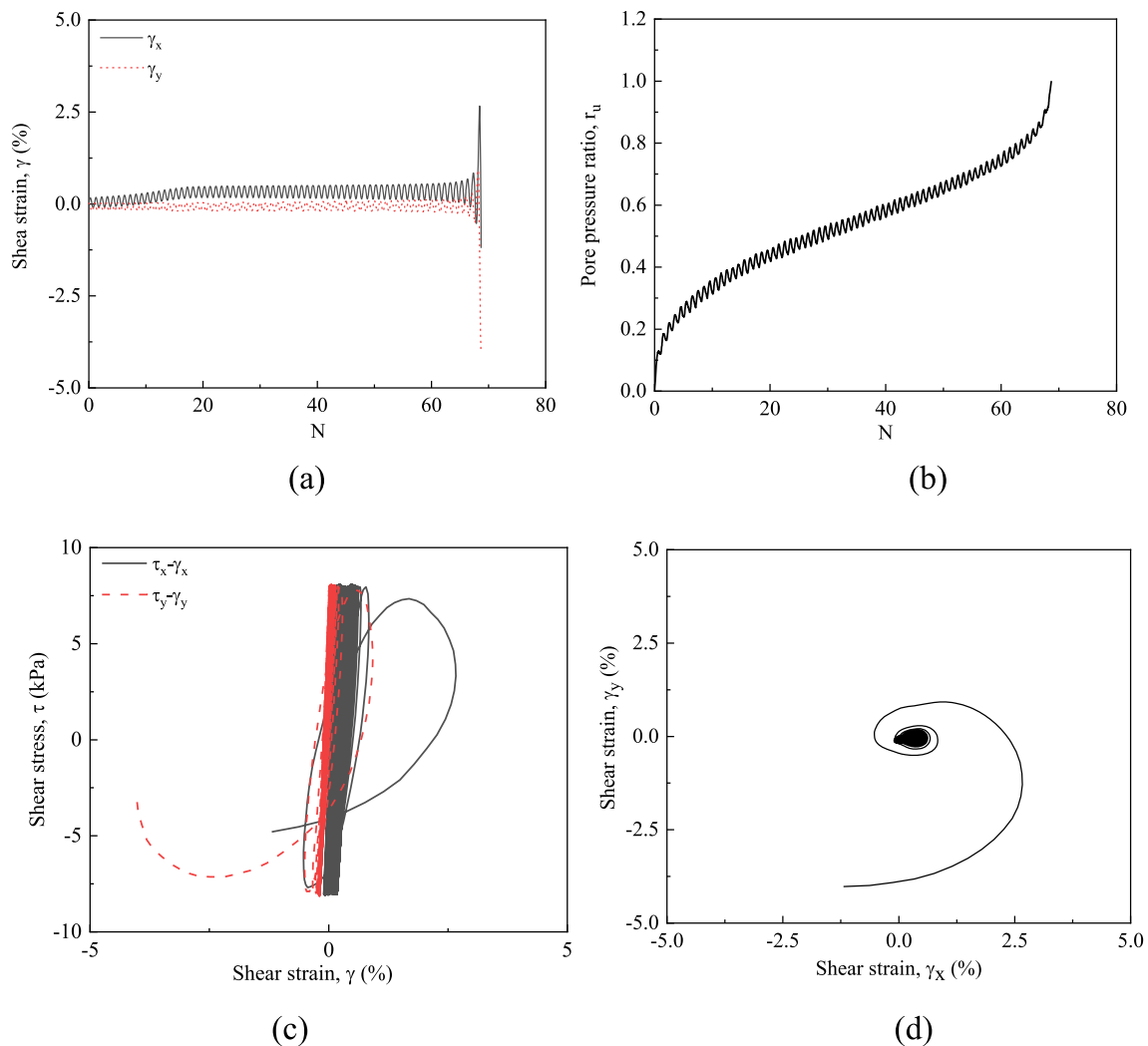


Fig. 6 Typical cyclic behaviors of unreinforced calcareous sand at CSR = 0.075: **a** variation of shear strain; **b** variation of pore pressure ratio; **c** shear stress–strain curve; **d** orbit of shear strain

along the left side of the σ'_v before reaching the transient peak points, and an instability line (IL) is plotted by connecting the transient peak points [25]. Meanwhile, the state of phase transformation is determined as the transient state from contractive to dilative behavior, and a phase transformation line (PTL) is also drawn by connecting the phase transformation points [21].

As reported in the existing research [7, 8, 26, 30, 50], the onset of liquefaction instability is commonly known as where the effective stress path intersects the IL. Furthermore, Alipour and Lashkari [1] revealed that loose granular soils were susceptible to pre-failure instability even when full drainage was granted, and two independent classes of instabilities may happen in granular soils. These results suggest that the onset of instability for sand can be predicted. Generally, liquefaction instability is expected to be triggered under cyclic loading when the cyclic stress path crosses the IL defined in the monotonic test and intercepts

the collapse surface considered as the locus defined by the corresponding monotonic effective stress path [2, 58]. Consequently, to investigate the linkage between monotonic and cyclic behaviors and determine the onset of liquefaction instability in cyclic tests, the IL established in the monotonic simple shear tests was superimposed on the typical cyclic effective stress paths (CSR = 0.075), as illustrated in Fig. 8c, d.

It is evident that during the early cycles, the σ'_v gradually decreases and approaches IL due to the accumulation of excess pore pressure. In the cycle following, when the cyclic stress paths cross the IL, the σ'_v presents a sudden decrease accompanied by pore water pressure and shear strain development rates sharply increase in both the unreinforced and fiber-reinforced specimens, signifying the initiation of the liquefaction instability. Moreover, compared to unreinforced calcareous sand fiber-reinforced sand requires more cycles to elicit unstable behaviors under

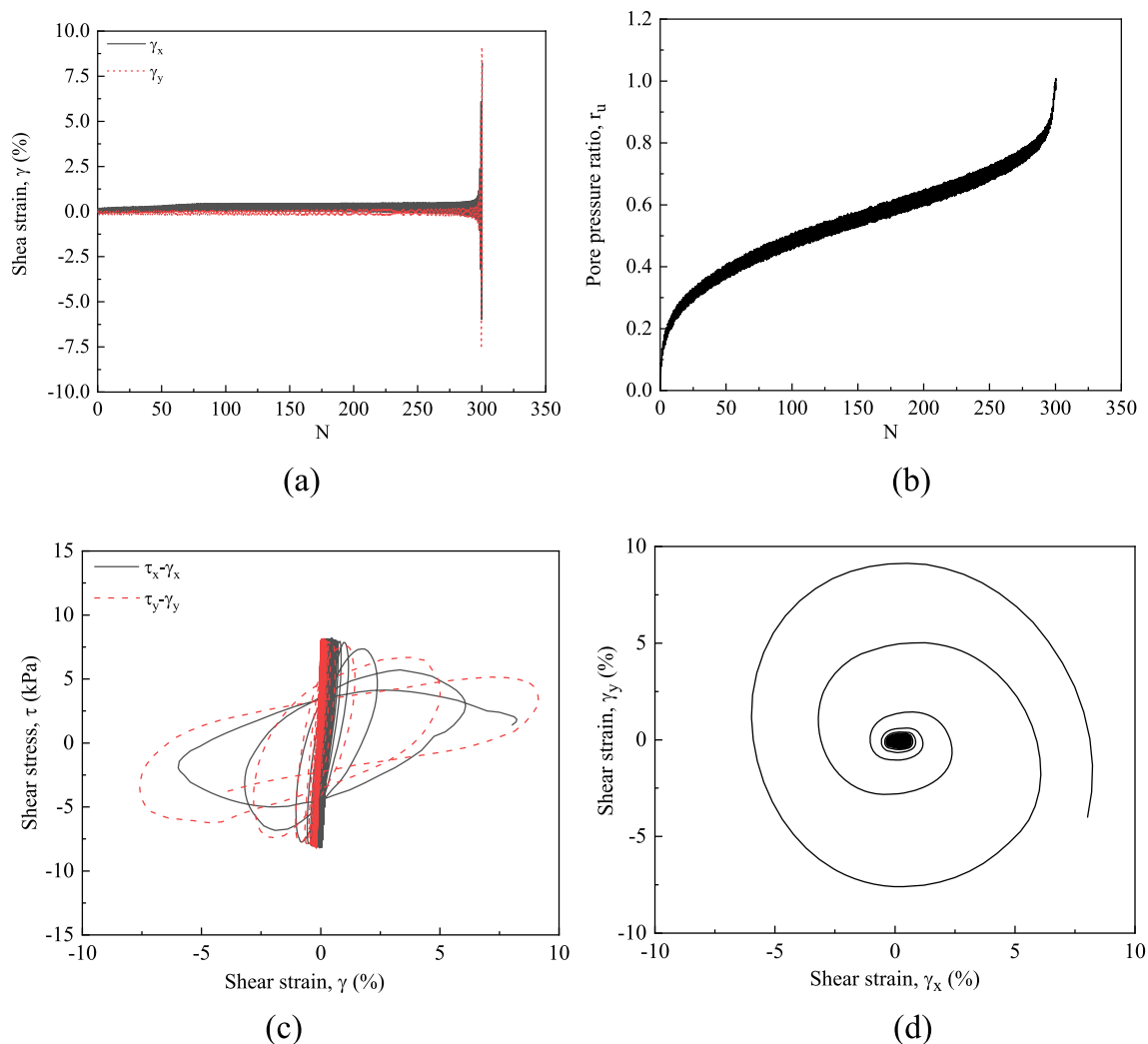


Fig. 7 Typical cyclic behaviors of fiber-reinforced calcareous sand with $\omega = 1\%$ at $\text{CSR} = 0.075$: **a** variation of shear strain; **b** variation of pore pressure ratio; **c** shear stress–strain curve; **d** orbit of shear strain

cyclic loading at the same initial vertical stress ($\sigma'_{v0} = 150$ kPa). This experimental phenomenon could be explained by the fact that the τ_p of fiber-reinforced sand is higher than the case of unreinforced sand under monotonic loading (IL or τ_p is significantly correlated with the cyclic behaviors), and the smaller τ_p will result in cyclic stress paths are more prone to touch the IL, thereby triggering liquefaction instability. Additionally, the *envelope effect* proposed by Li et al. [32] that the closer distance between the cyclic stress path and the monotonic stress path will lead to a higher decrease rate of the effective vertical stress is another factor responsible for more susceptibility to induce instability state in unreinforced sand (fiber-reinforced calcareous sand has a larger distance between monotonic and cyclic stress paths under the same loading conditions).

3.4 Liquefaction resistance

To investigate the effect of ω on the liquefaction resistance of calcareous sand, Fig. 9 shows the variation of N_L with ω for unreinforced and fiber-reinforced calcareous sand under multidirectional loading with a circular shear stress path at $\sigma'_{v0} = 150$ kPa. It can be found that N_L increases with the increase in ω , indicating that the liquefaction resistance of calcareous sand gradually improves. This is because the progressive increase in fibers in the specimen further reduces the build-up rate of pore pressure in calcareous sand, thereby enhancing the liquefaction resistance of fiber-reinforced calcareous sand.

Figure 10 depicts the curves of CSR with respect to N_L for calcareous sand in accordance with and without the existence of fiber. The figure clearly shows that the liquefaction resistance of calcareous sand decreases with an increase in CSR. Saxena et al. [47] revealed that there was

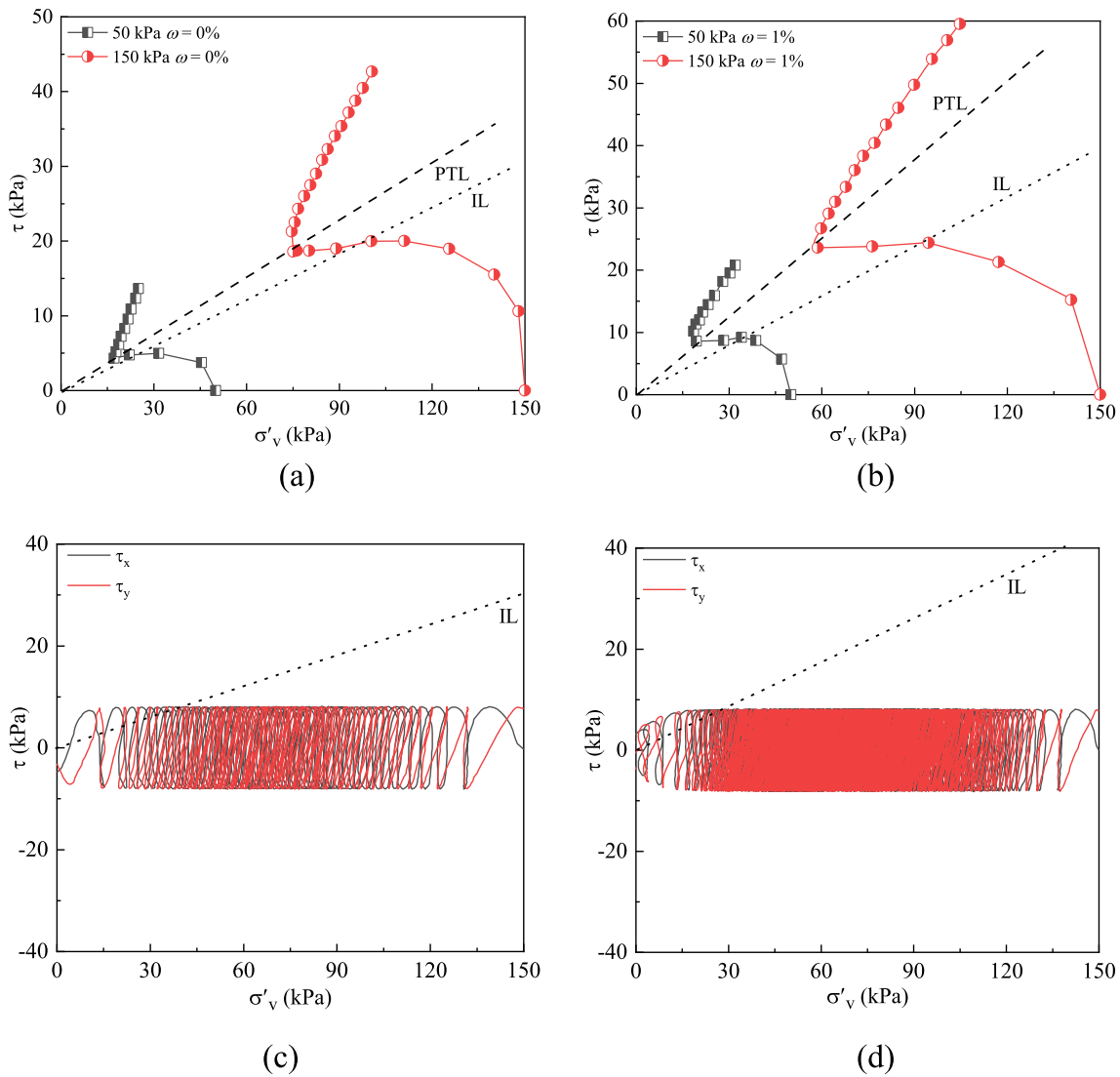


Fig. 8 Typical effective stress paths: **a** unreinforced sand under monotonic loading; **b** fiber-reinforced sand with $\omega = 1\%$ under monotonic loading; **c** unreinforced sand under cyclic loading at $CSR = 0.075$; **d** fiber-reinforced sand with $\omega = 1\%$ under cyclic loading at $CSR = 0.075$

a meaningful relationship between CSR and N_L for sand based on a series of experimental results as follows:

$$CSR = a \cdot N_L^{-b} \tag{2}$$

where a and b are test parameters related to the soil properties, generally determined by experiments. In this study, tests were conducted under different ω conditions, therefore, the variation of parameters a and b primarily relied on ω . Based on the fitting analysis of the experimental data, it can be found that the increase in ω has little effect on the value of parameter b which is always a constant ($b = 0.18$). However, as shown in Fig. 11, parameter a is significantly influenced by ω , and the relationship between parameter a and ω can be expressed as follows:

$$a = 4.0124 \cdot \omega + 0.1654 \tag{3}$$

subsequently, Eq. (4) can be acquired by introducing the relationship $a = 4.0124\omega + 0.1654$, $b = 0.18$ into Eq. (2) as follows:

$$CSR = (4.0124 \cdot \omega + 0.1654) \cdot N_L^{-0.18} \tag{4}$$

As illustrated in Fig. 10, the liquefaction resistance of fiber-reinforced calcareous sand with various ω can be well predicted by Eq. (4). To further reflect the effect of ω on N_L , the liquefaction resistance of fiber-reinforced calcareous sand is normalized, and the Eq. (4) is transformed as follows:

$$CSR / (4.0124 \cdot \omega + 0.1654) = N_L^{-0.18} \tag{5}$$

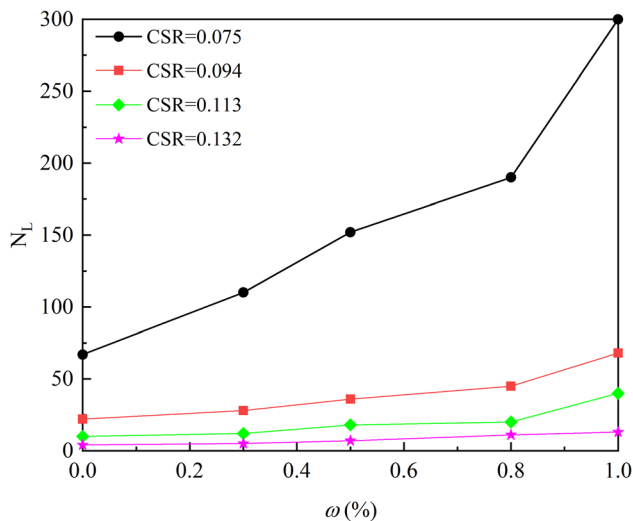


Fig. 9 N_L versus ω under multidirectional loading with a circular shear stress path at $\sigma'_{v0} = 150$ kPa

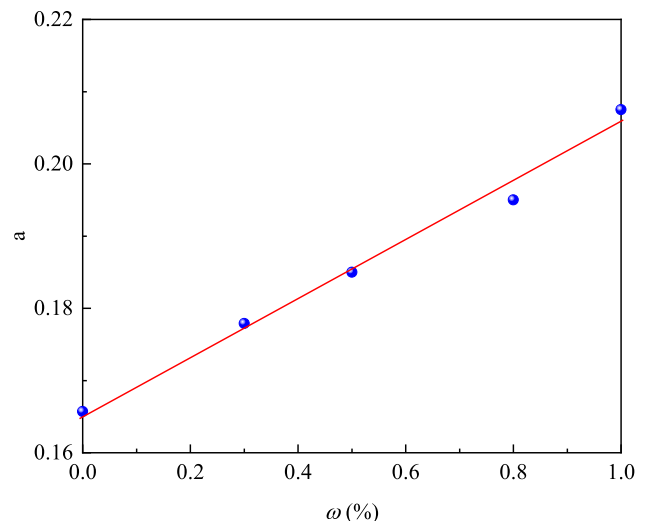


Fig. 11 Relationship between parameter a and ω

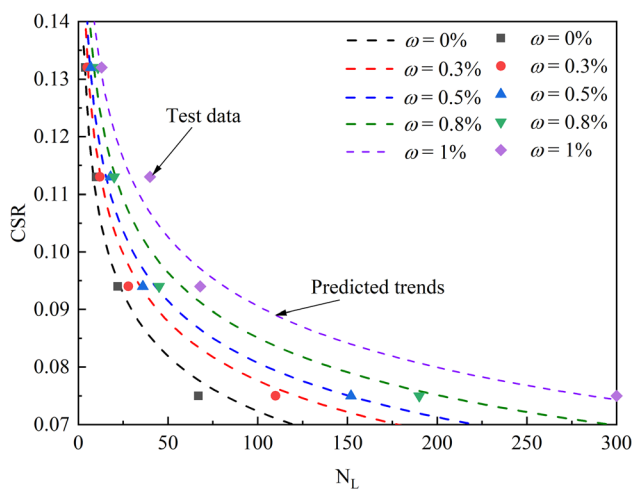


Fig. 10 Comparison between test data and the predicted values for liquefaction resistance of calcareous sand under various ω

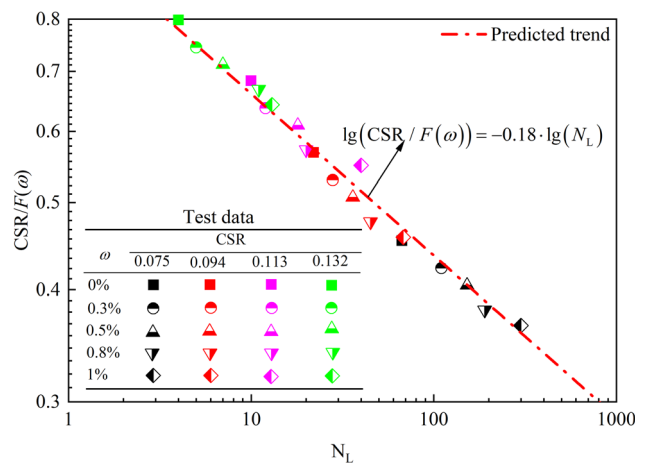


Fig. 12 Comparison between test data and the predicted values for normalized liquefaction resistance of calcareous sand under various ω

afterwards, making $F(\omega) = 4.0124\omega + 0.1654$, the development curve of normalized liquefaction resistance for fiber-reinforced calcareous sand is drawn by taking $CSR/F(\omega)$ as the vertical coordinate, and N_L as the horizontal coordinate, as shown in Fig. 12. It can be observed from Fig. 12 that all experimental data under various ω overlap on the same line (linear relationship) and can be expressed as follows:

$$\lg(CSR/F(\omega)) = -0.18 \cdot \lg(N_L) \quad (6)$$

Based on the linear relationship, the prediction of liquefaction resistance of calcareous sand with various ω can be achieved in a simple way, which will offer great convenience to engineering design on fiber-reinforced calcareous sand.

3.5 Pore pressure

Figure 13a displays the time histories of the pore pressure ratio under multidirectional loading with a circular shear stress path at $\sigma'_{v0} = 150$ kPa. It can be seen that increasing CSR from 0.075 to 0.132 significantly accelerates the accumulation rate of pore pressure. However, with increasing ω the build-up rate of pore pressure decreases, as shown in Fig. 13b. This is because the fibers reduce the deformation and permeability of specimens, thereby restricting the development of pore pressure. As an example, the accumulation rate of pore pressure for cohesive soil is extremely slow due to its poor permeability compared to sandy soil, which results in non-liquefiable properties of cohesive soil.

The residual pore pressure is defined as the pore pressure at the end of each cycle of loading where the applied

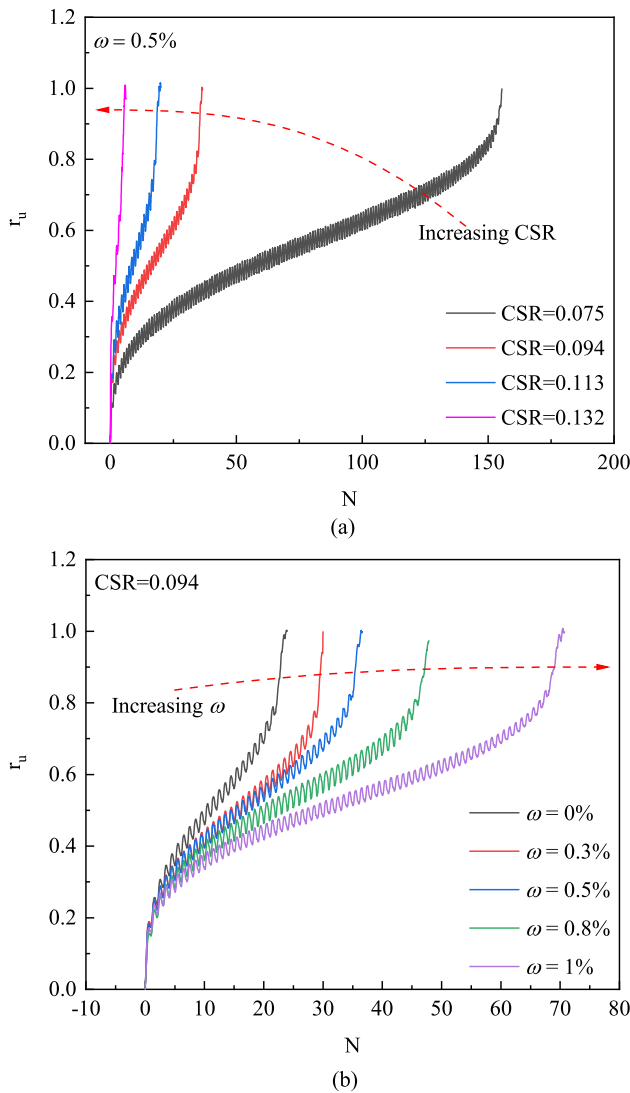


Fig. 13 Variation of pore pressure ratio under multidirectional loading with a circular shear stress path at $\sigma'_{v0} = 150$ kPa: **a** effect of CSR; **b** effect of ω

cyclic stress is restored to zero [11] and has a considerable influence on the effective stress acting on the soil. As shown in Fig. 14, the residual pore pressure is normalized to the initial vertical stress (i.e., $U = u_r/\sigma'_{v0}$) and then, plots against the current cycle normalized by the number of cycles to liquefaction (i.e., N/N_L). To investigate the difference in pore pressure behaviors between calcareous sand and quartz sand under cyclic shear loading, Fig. 14 shows the development features in terms of normalized residual pore pressure generation between different kinds of sand. It can be observed that the normalized residual pore pressure of fiber-reinforced calcareous sand is out of the range of quartz sand given by Lee et al. [31]. Similar findings can also be found in some research on calcareous sand [44]. To quantitatively describe the normalized residual pore pressure generation trend of the quartz sand, previous

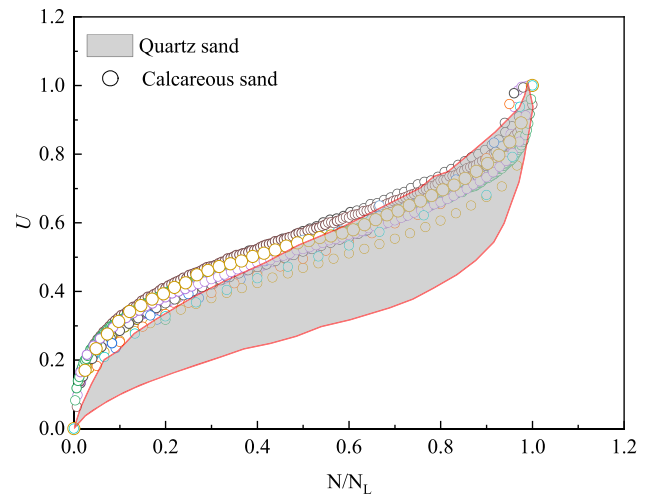


Fig. 14 Comparison of evolution pattern of normalized residual pore pressure ratio for different sands

researchers have established a range of pore pressure prediction models [41, 49]. Thus, whether the residual pore pressure prediction model concluded from tests conducted on quartz sand is valid in fiber-reinforced calcareous sand and proposing a prediction model applicable to fiber-reinforced calcareous sand requires further investigation.

Seed et al. [49] proposed an empirical model that has been widely accepted to simulate the pore pressure development trend of sand through extensive stress-controlled undrained cyclic tests as follows:

$$\frac{\Delta u_r}{p_0} = \frac{2}{\pi} \arcsin \left(\frac{N}{N_L} \right)^{\frac{1}{2\alpha}} \tag{7}$$

where $\Delta u_r/p_0$ is the normalized residual pore pressure after N number of loading cycles, and α is the empirical constant. Figure 15 shows the comparison of test results for

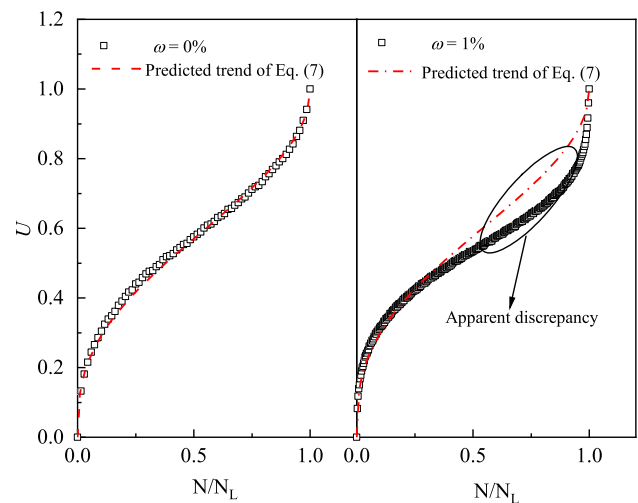


Fig. 15 Comparison between test data and predicted trend of Eq. (7)

unreinforced calcareous sand with the predicted trend using Eq. (7). It can be found that the prediction model can be used to simulate the general tendency of pore pressure evolution for unreinforced calcareous sand although the model was obtained from quartz sand. The result demonstrates the widespread applicability of the model proposed by Seed et al. [49]. However, the discrepancy between this model and the experimental data of the present study increases with the increase in ω , especially for $\omega = 1\%$ as illustrated in Fig. 15, which indicates that the inclusion of fibers has a greater influence on the development of residual pore pressure, and the pore pressure prediction model proposed by Seed et al. [49] cannot reflect the effect of fibers. Equation (7) overestimates the normalized residual pore pressure development of fiber-reinforced calcareous sand with $\omega = 1\%$ at larger N/N_L . In fact, compared to clean quartz sand the soil properties of fiber-reinforced calcareous sand are more complex; thus, appropriately increasing empirical parameters in the prediction model is necessary. Considering that the inverse trigonometric function can relatively well fit the reverse S curve and the power function can change the shape of the curve, a modified normalized residual pore pressure prediction model with two empirical parameters was proposed, which can reflect the effect of fibers as follows:

$$U = \frac{2}{\pi} \arcsin \left(\frac{N}{N_L} \right)^{a(N/N_L)^{2b} + b + (N/N_L)^{10}} \quad (8)$$

where a and b denote two empirical parameters that can be calibrated by undrained cyclic tests.

Figure 16 gives the comparison of test results for normalized residual pore pressure with the predicted trend using Eq. (8). It can be found that the development trend of residual pore pressure can be well predicted with this

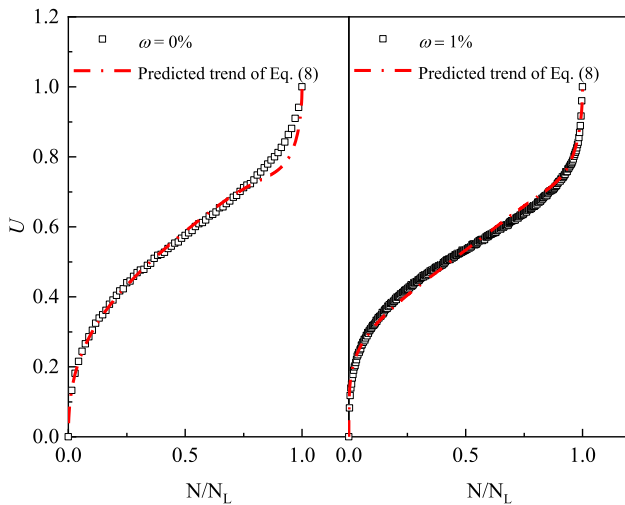
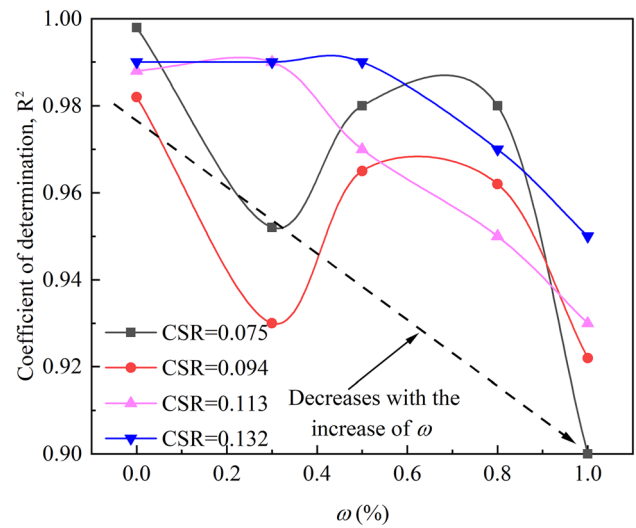
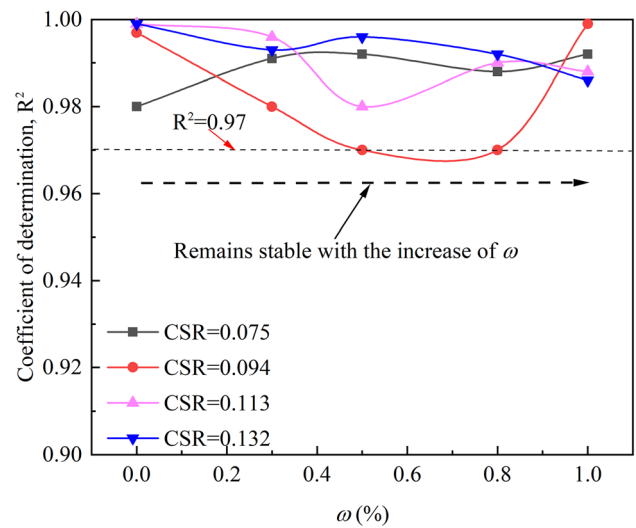


Fig. 16 Comparison between test data and predicted trend of Eq. (8)

proposed model under unreinforced and fiber-reinforced conditions. To highlight the applicability of the proposed model, Fig. 17 depicts the curves of coefficient of determination (R^2) versus ω for various residual pore pressure prediction models. The coefficient of determination for Eq. (7) decreases with an increase in ω (i.e., decreases from 0.99 to 0.9 as ω increases), whereas the coefficient of determination for Eq. (8) is basically greater than 0.97 and is independent of the variation of ω . The results indicate that the proposed prediction model in this study can better simulate the development trend of normalized residual pore pressure of fiber-reinforced calcareous sand with various ω under undrained conditions compared with Eq. (7).



(a)



(b)

Fig. 17 Coefficient of determination for various normalized residual pore pressure prediction models versus ω : a Eq. (7); b Eq. (8)

4 Conclusions

A series of undrained monotonic and multidirectional cyclic simple shear tests were conducted to investigate the effects of cyclic stress ratios and fiber contents on the responses of calcareous sand. The peak shear strength, the linkage between monotonic and cyclic behaviors, liquefaction resistance and pore pressure of unreinforced and fiber-reinforced calcareous sand were analyzed. The following conclusions are drawn from this study.

- (1) In the monotonic shear tests, both the unreinforced and fiber-reinforced calcareous sand exhibit limited flow instability behavior, and the peak shear strength and phase transformation shear strength increase with the increase in fiber content. A more pronounced reinforcement efficiency of increasing fiber content in improving peak shear strength can be found in a smaller initial vertical stress.
- (2) When the cyclic effective stress paths cross the instability line determined in the monotonic tests, the effective vertical stress presents a sudden decrease accompanied by pore water pressure and shear strain development rates sharply increase in both the unreinforced and fiber-reinforced specimens. Compared to unreinforced calcareous sand, fiber-reinforced sand requires more cycles to elicit unstable behaviors under cyclic loading due to the larger peak shear strength.
- (3) The liquefaction resistance of calcareous sand increases with the increase in fiber contents; however, increasing the cyclic stress ratio reduces the liquefaction resistance of calcareous sand. A linear relationship is found between the normalized liquefaction resistance of fiber-reinforced sand and the number of cycles for triggering liquefaction, which provides a convenient way to predict the liquefaction resistance of calcareous sand with various fiber contents.
- (4) The build-up rate of pore pressure decreases as fiber contents increases, whereas increasing the cyclic stress ratio significantly accelerates the accumulation rate of pore pressure. A modified normalized residual pore pressure prediction model which can reflect the effects of fibers is proposed in this study. Compared to the widely used Seed model, the proposed prediction model can better simulate the pore pressure development trend of fiber-reinforced calcareous sand with various fiber contents.

It has to be noted that these findings were concluded from experiments with fixed initial vertical stress and circular shear stress path, whereas the real conditions of soils

and shear stress path during earthquakes were more complex than the simple shear conditions considered in this study. Nevertheless, the results of the experiments conducted under these limited conditions have indicated that fiber reinforcement can greatly improve the performance of calcareous sand even under multidirectional cyclic shear loading.

Acknowledgements The authors appreciate the financial support provided by the National Natural Science Foundation of China (NSFC) (Grant Nos. 41772289 & 41572266).

Funding National Natural Science Foundation of China, Grant/Award Number: 41772289. National Natural Science Foundation of China, Grant/Award Number: 41572266.

Availability of data and materials The data underlying this article will be shared on reasonable request to the corresponding author.

Declarations

Conflict of interest The authors have no conflicts of interest to declare that are relevant to the content of this article.

References

1. Alipour MJ, Lashkari A (2018) Sand instability under constant shear drained stress path. *Int J Solids Struct* 150:66–82
2. Andrade JE, Ramos AM, Lizcano A (2013) Criterion for flow liquefaction instability. *Acta Geotech* 8(5):525–535
3. Behzad Fatahi HR (2021) Liquefaction and post-liquefaction resistance of sand reinforced with recycled geofibre. *Geotext Geomembr* 50(1):69–81
4. Boominathan A, Hari S (2002) Liquefaction strength of fly ash reinforced with randomly distributed fibers. *Soil Dyn Earth Eng* 22(9):1027–1033
5. Chegenizadeh A, Keramatikerman M, Nikraz H (2018) Liquefaction resistance of fibre reinforced low-plasticity silt. *Soil Dyn Earthq Eng* 104:372–377
6. Chen GX, Liang K, Zhao K, Yang J (2022) Shear modulus and damping ratio of saturated coral sand under generalised cyclic loadings. *Géotechnique*. <https://doi.org/10.1680/jgeot.21.00181>
7. Chu J, Leroueil S, Leong WK (2003) Unstable behavior of sand and its implication for slope stability. *Can Geotech J* 40(5):874–885
8. Chu J, Wanatowski D (2009) Effect of loading mode on strain softening and instability of sand in plain-strain tests. *J Geotech Geoenviron Eng* 135(1):108–120
9. Correia NS, Rocha SA, Lodi PC, McCartney JS (2021) Shear strength behavior of clayey soil reinforced with polypropylene fibers under drained and undrained conditions. *Geotext Geomembr* 49(5):1419–1426
10. Ding G, Zhou L, Wang J, Xu Y, Li X (2020) Shaking table tests on gravel slopes reinforced by concrete canvas. *Geotext Geomembr* 48(4):539–545
11. Dobry R, Ladd R, Yokel FY, Chung RM, Powell D (1982) Prediction of pore water pressure buildup and liquefaction of sands during earthquakes by the cyclic strain method. National Bureau of Standards, Gaithersburg, MD
12. Dyvik R, Berre T, Lacasse S, Raadim B (1987) Comparison of truly undrained and constant volume direct simple shear tests. *Géotechnique* 37(1):3–10

13. EdinLiler A, Toksoy YS (2016) Physical model study of the seismic performance of highway embankments with and without geotextile. *J Earthq Tsunami* 11(2):1750003
14. El-Emam MM, Bathurst RJ (2007) Influence of reinforcement parameters on the seismic response of reduced-scale reinforced soil retaining walls. *Geotext Geomembr* 25(1):33–49
15. Falorca MCFG, Pinto MIM (2011) Effect of short, randomly distributed, polypropylene microfibrils on shear strength behaviour of soils. *Geosynth Int* 18(1):1–11
16. Ghadr S, Samadzadeh A, Bahadori H, Langroudi AA (2020) Liquefaction resistance of fibre-reinforced silty sands under cyclic loading. *Geotext Geomembr* 48(6):812–827
17. Hamidi A, Hooresfand M (2013) Effect of fiber reinforcement on triaxial shear behavior of cement treated sand. *Geotext Geomembr* 36(1):1–9
18. Huang CC (2019) Seismic responses of vertical-faced wrap-around reinforced soil walls. *Geosynth Int* 26(2):146–163
19. Hyodo M, Hyde AFL, Aramaki N (1998) Liquefaction of crushable soils. *Geotechnique* 48(4):527–543
20. Ibraim E, Diambra A, Muir Wood D, Russell AR (2010) Static liquefaction of fibre reinforced sand under monotonic loading. *Geotext Geomembr* 28(4):374–385
21. Ishihara K, Tatsuoaka F, Yasuda S (1975) Undrained deformation and liquefaction of sand under cyclic stresses. *Soils Found* 15(1):29–44
22. Ishihara K, Yamazaki F (1980) Cyclic simple shear tests on saturated sand in multi-directional loading. *Soils Found* 20(1):45–59
23. Jin H, Guo L (2021) Effect of phase difference on the liquefaction behavior of sand in multidirectional simple shear tests. *J Geotech Geoenviron Eng* 147(2):06021015
24. Komak Panah A, Yazdi M, Ghalandarzadeh A (2015) Shaking table tests on soil retaining walls reinforced by polymeric strips. *Geotext Geomembr* 43:148–161
25. Lade PV (1993) Initiation of static instability in the submarine Nerlerk Berm. *Can Geotech J* 30(6):895–904
26. Lade PV, Nelson RB, Ito YM (1988) Instability of granular materials with nonassociated flow. *J Eng Mech* 114(12):2173–2191
27. Lashkari A, Falsafizadeh SR, Rahman M (2021) Influence of linear coupling between volumetric and shear strains on instability and post-peak softening of sand in direct simple shear tests. *Acta Geotech* 16(11):3467–3488
28. Lashkari A, Falsafizadeh SR, Shourijeh PT, Alipour MJ (2020) Instability of loose sand in constant volume direct simple shear tests in relation to particle shape. *Acta Geotech* 15(9):2507–2527
29. Lashkari A, Shourijeh PT, Khorasani SSS, Irani N, Rahman MM (2022) Effects of over-consolidation history on flow instability of clean and silty sands. *Acta Geotech*. <https://doi.org/10.1007/s11440-022-01502-y>
30. Lashkari A, Yaghtin MS (2018) Sand flow liquefaction instability under shear-volume coupled strain paths. *Géotechnique* 68(11):1002–1024
31. Lee KL, Albaisa A (1974) Earthquake induced settlements in saturated sands. *J Geotech Eng Div* 100(4):387–406
32. Li Y, Yang Y, Yu HS, Roberts G (2017) Correlations between the stress paths of a monotonic test and a cyclic test under the same initial conditions. *Soil Dyn Earthq Eng* 101:153–156
33. Li Y, Yang Y, Yu HS, Roberts G (2017) Monotonic direct simple shear tests on sand under multidirectional loading. *Int J Geomech* 17(1):04016038
34. Lin YL, Leng WM, Yang GL, Li L, Yang JS (2015) Seismic response of embankment slopes with different reinforcing measures in shaking table tests. *Nat Hazards* 76(2):791–810
35. Ling HI, Leshchinsky D, Mohri Y, Wang JP (2012) Earthquake response of reinforced segmental retaining walls backfilled with substantial percentage of fines. *J Geotech Geoenviron Eng* 138(8):934–944
36. Liu J, Hou T, Luo Y, Cui Y (2020) Experimental study on unconsolidated undrained shear strength characteristics of synthetic cotton fiber reinforced soil. *Geotech Geol Eng* 38(10):1773–1783
37. Liu J, Wang G, Kamai T, Zhang F, Yang J, Shi B (2011) Static liquefaction behavior of saturated fiber-reinforced sand in undrained ring-shear tests. *Geotext Geomembr* 29(5):462–471
38. Lovisa JS, Shukla SK, Sivakugan N (2010) Shear strength of randomly distributed moist fibre-reinforced sand. *Geosynth Int* 17(2):100–106
39. Maheshwari BK, Singh HP, Saran S (2012) Effects of reinforcement on liquefaction resistance of Solani sand. *J Geotech Geoenviron Eng* 138(7):831–840
40. Noorzad R, Amini Fardad P (2014) Liquefaction resistance of babolsar sand reinforced with randomly distributed fibers under cyclic loading. *Soil Dyn Earthq Eng* 66:281–292
41. Pan K, Yang ZX (2018) Effects of initial static shear on cyclic resistance and pore pressure generation of saturated sand. *Acta Geotech* 13(2):473–487
42. Park T, Ann Tan S (2005) Enhanced performance of reinforced soil walls by the inclusion of short fiber. *Geotext Geomembr* 23(4):348–361
43. PHRI (1997) Handbook on liquefaction remediation of reclaimed land. Port and Harbor Research Institute Balkema, Rotterdam
44. Porcino DD, Tomasello G (2019) Shear wave velocity-based evaluation of liquefaction resistance for calcareous sands of different origin. *Soil Dyn Earthq Eng* 122:235–247
45. Pyke R, Seed H, Chan C (1975) Settlement of sands under multidirectional shaking. *J Geotech Eng* 101(GT4):379–398
46. Salem M, Elmamlouk H, Agaiby S (2013) Static and cyclic behavior of north coast calcareous sand in Egypt. *Soil Dyn Earth Eng* 55(12):83–91
47. Saxena SK, Reddy KR, Avramidis AS (1988) Liquefaction resistance of artificially cemented sand. *J Geotech Eng* 114(12):1395–1413
48. Seed B, Lee KL (1966) Liquefaction of saturated sands during cyclic loading. *J Soil Mech Found Div* 92:105–134
49. Seed HB, Martin PP, Lysmer J (1975) The generation and dissipation of pore water pressures during soil liquefaction. Report No. EERC 75-26. University of California, Berkeley, CA
50. Slade JA, Hollande RDD, Krahn J (1985) The liquefaction of sands, a collapse surface approach. *Can Geotech J* 22(4):564–578
51. Srilatha N, Latha GM, Puttappa CG (2013) Effect of frequency on seismic response of reinforced soil slopes in shaking table tests. *Geotext Geomembr* 36(2):27–32
52. Su D, Li XS (2008) Impact of multidirectional shaking on liquefaction potential of level sand deposits. *Geotechnique* 58(4):259–267
53. Vaid YP, Stedman JD, Sivathayalan S (2001) Confining stress and static shear effects in cyclic liquefaction. *Can Geotech J* 38(3):580–591
54. Wang L, Chen G, Chen S (2015) Experimental study on seismic response of geogrid reinforced rigid retaining walls with saturated backfill sand. *Geotext Geomembr* 43(1):35–45
55. Wang XZ, Jiao YY, Wang R, Hu MJ, Meng QS, Tan FY (2011) Engineering characteristics of the calcareous sand in Nansha Islands, South China Sea. *Eng Geol* 120(1–4):40–47
56. Wang G, Wang ZN, Ye QG, Wei X (2020) Particle breakage and deformation behavior of carbonate sand under drained and undrained triaxial compression. *Int J Geomech* 20(3):04020012
57. Xiao P, Liu H, Yang X, Stuedlein AW, Evans TM (2018) Liquefaction resistance of bio-cemented calcareous sand. *Soil Dyn Earthq Eng* 107:9–19

58. Yang Z, Pan K (2017) Flow deformation and cyclic resistance of saturated loose sand considering initial static shear effect. *Soil Dyn Earthq Eng* 92(1):68–78
59. Yazdandoust M (2017) Investigation on the seismic performance of steel-strip reinforced-soil retaining walls using shaking table test. *Soil Dyn Earthq Eng* 97:216–232
60. Ye B, Cheng Z, Liu C, Zhang Y, Lu P (2017) Liquefaction resistance of sand reinforced with randomly distributed polypropylene fibres. *Geosynth Int* 24(6):625–636
61. Yüncül K, Gürbüz A (2021) Shaking table study on seismic behavior of MSE wall with inclined backfill soils reinforced by polymeric geostrips. *Geotext Geomembr* 50(1):116–136
62. Zhang XD, Russell AR (2021) Liquefaction potential and effective stress of fiber-reinforced sand during undrained cyclic loading. *J Geotech Geoenviron Eng* 147(7):04021042
63. Zhang J, Yang Z, Yang Q, Yang G, Li G, Liu J (2021) Liquefaction behavior of fiber-reinforced sand based on cyclic triaxial tests. *Geosynth Int* 28(3):316–326
64. Zhou L, Ding GY (2021) Seismic response of reinforced retaining walls with saturated calcareous sand backfill subjected to acid rain erosion. *J Mater Civ Eng* 33(8):06021005
65. Zhou L, Ding G, Tan J, Zhao XX, Wang J (2020) Seismic response of concrete-canvas reinforced slopes: influence of tilt degrees for reinforcement. *J Earthq Tsunami* 14(3):2050011

Publisher's Note Springer Nature remains neutral with regard to jurisdictional claims in published maps and institutional affiliations.

Springer Nature or its licensor (e.g. a society or other partner) holds exclusive rights to this article under a publishing agreement with the author(s) or other rightsholder(s); author self-archiving of the accepted manuscript version of this article is solely governed by the terms of such publishing agreement and applicable law.